https://doi.org/10.5194/hess-2019-696
Preprint. Discussion started: 3 February 2020

Hydrology and Earth System Sciences
Discussions

Assimilating Shallow Soil Moisture Observations into Land Models with a Water Budget Constraint

Bo Dan[1], Xiaogu Zheng[2], Guocan Wu[3*], and Tao Li[4]

[1] National Marine Data and Information Service, Tianjin, China

[2]Key Laboratory of Regional Climate-Environment Research for East Asia, Institute of Atmospheric Physics, Chinese Academy of Sciences, Beijing, China

[3]College of Global Change and Earth System Science, Beijing Normal University, Beijing, China

[4]Institute of Statistics, Xi'an University of Finance and Economics, Xi'an, China

*Corresponding author: Guocan Wu
E-mail: gcwu@bnu.edu.cn

Abstract

Incorporating observations of shallow soil moisture content into land models is an important step in assimilating satellite observations of soil moisture content. In this study, several modifications of an ensemble Kalman filter (EnKF) are proposed for improving this assimilation. It was found that a forecast error inflation-based approach improves the soil moisture content in shallow layers, but it can increase the analysis error in deep layers. To mitigate the problem in deep layers while maintaining the improvement in shallow layers, a vertical localization-based approach was introduced in this study. During the data assimilation process, although updating the forecast state using observations can reduce the analysis error, the water balance based on the physics in the model could be destroyed. To alleviate the imbalance in the water budget, a weak water balance constrain filter is adopted.

The proposed weakly constrained EnKF that includes forecast error inflation and vertical localization was applied to a synthetic experiment and two real data experiments. The results of the assimilation process suggest that the inflation approach effectively reduce both the short-lived analysis error and the analysis bias in shallow layers, while the vertical localization approach avoids increase in analysis error in deep layers. The weak constraint on the water balance reduces the degree of the water budget imbalance at the price of a small increase in the analysis error.

Keywords

soil moisture, water balance, data assimilation, forecast error inflation, vertical localization

1. Introduction

Soil moisture content is one of the most important variables that affect the water cycle and energy balance through land-atmosphere interactions, especially evaporation and precipitation (Han et al. 2014; Kumar et al. 2014; McColl et al. 2019; Pinnington et al. 2018). Adequate knowledge of the horizontal and vertical distributions of soil moisture could improve weather and climate predictions (Delworth and Manabe 1988; Pielke 2001). Alongside snow cover, soil moisture content is an important component of the meteorological memory of the climate system over land (McColl et al. 2019; Robock et al. 2000; Zhao and Yang 2018). It is also a primary water resource for the terrestrial ecosystem and affects runoff (GUSEV and Novak 2007).

There are several ways to estimate the soil moisture content. Land surface models can provide temporally and spatially continuous estimates of the soil moisture content, but these estimates are limited by the uncertainty in the models' parameters, errors in the forcing data and imperfect physical parameterizations (Bonan 1996; Dai et al. 2003; Dickinson et al. 1993; Oleson et al. 2010; Yang et al. 2009). Compared with the results of models, in-situ observations of the soil moisture content provide more accurate profiles (Bosilovich and Lawford 2002; Dorigo et al. 2011; Robock et al. 2000); however, networks of in-situ observations are usually too sparse to estimate the soil moisture content on a regional scale (Gruber et al. 2018; Loizu et al. 2018). Satellite remote sensing retrievals could provide soil moisture content data on regional scales (Bartalis et al. 2007; Crow et al. 2017; Entekhabi et al. 2010; Kerr et al. 2010; Lu et al. 2015; Njoku et al. 2003), but they are only available for the shallow layer of the soil and the quality is poor in vegetated area (Pinnington et al. 2018; Yang et al. 2009).

https://doi.org/10.5194/hess-2019-696
Preprint. Discussion started: 3 February 2020

A much better approach to improving estimates of soil moisture contents on regional scales is to constrain land model prediction by assimilating data from large-scale remote sensing observations of the soil moisture content (Crow and Loon 2006; Crow and Wood 2003; Reichle and Koster 2005). The assimilation of passive microwave measurements (brightness temperatures) into land surface models can successfully increases the spatial and temporal coverage by interpolation and extrapolation to unobserved times and locations, and also provide various land surface state and flux estimates with reduced uncertainty (De Lannoy and Reichle 2016; Reichle et al. 2017). Therefore, land surface data assimilation has significantly improved the utility of surface soil moisture data sets (Crow et al. 2017; Lu et al. 2012; Lu et al. 2015), and can further improve land surface model initial conditions for coupled short-term weather prediction (Chen et al. 2014; Santanello et al. 2016; Yang et al. 2016).

A good estimate of the forecast error covariance matrix is crucial for the compromise between uncertain observations and imperfect model predictions in data assimilation (Anderson and Anderson 1999; Miyoshi 2011; Miyoshi et al. 2012; Wang and Bishop 2003). For the Ensemble Kalman Filter (EnKF) assimilation method, the forecast error covariance matrix is estimated using the sample covariance matrix of the ensemble forecasts (Dumedah and Walker 2014; Evensen 1994; Han et al. 2014). However, it is usually underestimated due to sampling and model errors, which can eventually results in filter divergence (Anderson and Anderson 1999; Constantinescu et al. 2007; Yang et al. 2015). To address this problem, it suggests that the forecast covariance matrix be multiplied by an inflation factor (Dee and Da Silva 1999; Dee et al. 1999; Li et al. 2012; Zheng 2009). This approach is referred to as inflation, and it becomes particularly important when the error in the model is large (Bauser et al.

https://doi.org/10.5194/hess-2019-696
Preprint. Discussion started: 3 February 2020

2018; El Gharamti et al. 2019; Liang et al. 2012; Raanes et al. 2019; Wu et al. 2013). Therefore, it could work well in this situation because of the enormous errors in the land model.

In this study, a scheme for assimilating synthetic and in-situ shallow observations of the soil moisture content into land models was developed based on EnKF method, which can provide a foundation for further satellite data assimilation. For the synthetic experiment, the CLM 4.0 (Version 4.0 of the Community Land Model, (Lawrence et al. 2011; Oleson et al. 2010)) was used to generate the "true values" and the CoLM (Common Land Model, (Dai et al, 2003)) was selected as the forecast operator. The differences in these two models are referred to the model error in an imperfect land surface model. The inflation factors are estimated at every observation time step during the assimilation process by minimizing the -2log-likelihood of the difference between the forecast and the observation (Liang et al. 2012; Zheng 2009). For assimilating observations near the surface only, such inflation approach can improve the estimates of the forecast error statistics in shallow soil layers but may artificially enlarge the forecast error statistics in deep soil layers. To avoid the possibility of decreasing the quality of the estimates in deep soil layers, a vertical localization with weighting of observations is adopted (Janjić et al. 2011). In this approach, a localization function multiplies the weights on the components of the state vector according to the distance from state layer to the observation. Moreover, the method based on the maximum likelihood estimation was proposed to estimate the optimal localization scale factor. These steps can result in a better prediction of the soil moisture content in the deep layers.

A major objective of soil moisture data assimilation is to address biases in models and observations (Koster et al. 2009; Reichle and Koster 2004). In this study,

https://doi.org/10.5194/hess-2019-696
Preprint. Discussion started: 3 February 2020

we only assume that models could be biased, while the soil moisture observations are assumed to be unbiased. Moreover, the soil moisture observations are restricted in shallow layer, so there is no observation available to correct the modeled soil moisture biases in deep layers. If one only removes the bias in shallow layer, it would introduce error in model dynamics. Therefore in this study, we still use traditional bias-blind data assimilation framework. Nevertheless, the analysis error is further decomposed to a short-lived error (random error) and a bias (system error). It demonstrates that the proposed scheme can reduce the both for soil moisture in shallow layer.

In addition to improve assimilation accuracy, this study also focuses on the imbalance in the water budget that occurs during the process of assimilating the soil moisture data. The terrestrial water budget is a key part of the global hydrologic cycle. A better understanding of the budget can help us to improve our knowledge of land-atmosphere water exchange and related physical mechanisms and therefore, can improve our ability to develop models (Pan and Wood 2006). Generally speaking, analyses do not conserve the water budget due to inconsistencies between predictions made by models and observations (Li et al. 2012; Pan and Wood 2006; Wei et al. 2010; Yilmaz et al. 2011; Yilmaz et al. 2012). It is really a problem if the water balance is violated in a systematic manner (for example, model is biased), which suggests a trouble in data assimilation. Pan and Wood (2006) proposed a method based on a strong constraint to reincorporate the water balance. However, this method redistributes the error among the different terms in the water budget, which could result in unrealistic estimates (Pan and Wood 2006; Yilmaz et al. 2011).

To overcome this shortcoming, Yilmaz et al. (2011) proposed using a weakly constrained ensemble Kalman filter (WCEnKF) to reduce the imbalance in the water budget. In a synthetic study, they concluded that the accuracy of a WCEnKF-based

https://doi.org/10.5194/hess-2019-696
Preprint. Discussion started: 3 February 2020

Hydrology and Earth System Sciences Discussions

analysis is close to that of an EnKF-based analysis but the water budget balance residuals are much smaller than that of an unconstrained filter. Nevertheless, the observations of the soil moisture content cover the entire column, and a perfect model was used in their studies. This is not generally true, especially when only satellite observations are assimilated. In this study, the experiments were further designed to assimilate surface observations into an imperfect land model.

The structure of this paper is arranged as follows: The data and models used in this study are described in section 2. The details of the WCEnKF-based method that incorporates inflation and vertical localization (WCEnKF-Inf-Loc) are provided in section 3. The experimental designs and evaluations of synthetic and real data experiments are set in sections 4 and 5. The primary results of the synthetic and real experiments are given in section 6. The discussion and conclusion comprise sections 7 and 8.

2. Models and data

2.1 Study area and in-situ stations

The study area is located in the Mongolian Plateau and comprises approximately 9352 square kilometers between 46° and 46.5°N and between 106.125° and 107°E. The dominant biome is grassland, and no river flows through the area (see Figure 1).

The soil moisture content and related meteorological and hydrological parameters are monitored by automatic stations maintained by the Coordinated Enhanced Observing Period Asian Monsoon Project (CEOP AP) (Bosilovich and Lawford 2002; Lawford et al. 2004). The CEOP AP was launched by the World Climate Research Programme (WCRP) to develop an integrated global dataset that can be used to address issues relating to water and energy budget simulations and predictions, monsoon processes and the prediction of river flows. More details can be found at http://www.ceop.net. In this study, observations of the soil moisture content from two stations, the Bayantsagaan Station (BTS 46.7765°N, 107.14228°E) and the Delgertsgot Station (DGS 46.12731°N, 106.36856°E), were used to validate the assimilation method. At the BTS, the soil moisture content is measured every half hour at 3, 10, 20 and 40 cm below the surface. At the DGS, measurements are made at depths of 3, 10, 40 and 100 cm with the same frequency. Only the observations made at 6:00 am (same with the overpass time of SMOS satellite) are assimilated, while the others are used for validation.

2.2 Forcing data

In this study, both synthetic and realistic experiments were conducted to explore the accuracy of the assimilation schemes. In the synthetic experiments, the simulations were driven by forcing data (including radiation, wind, pressure, humidity, precipitation and temperature) from the 0.125°x0.125° ERA-Interim dataset (Dee et al. 2011) that had been scaled down to provide a temporal resolution of one hour.

In the realistic experiments, the forcing data comprised hourly measurements of the wind speed, near-surface air temperature, relative humidity precipitation and surface pressure at local stations (the BTS and DGS). The downward shortwave and longwave radiation data used were from model output time series data for the study area provided by the Japanese Meteorological Agency (Huang et al. 2008).

2.3 Models

The Common Land Model (CoLM) developed by Dai et al. (2003) is a third-generation land surface model. It combines the best features of three successful

https://doi.org/10.5194/hess-2019-696
Preprint. Discussion started: 3 February 2020

models: the Land Surface Model (LSM, (Bonan 1996)), the Biosphere-Atmosphere Transfer Scheme (BATS, (Dickinson et al. 1993)) and the 1994 version of the Chinese Academy of Sciences/Institute of Atmospheric Physics model (IAP94, (Dai et al. 2003)), and is being further developed. The primary characteristics of the model include 10 unevenly spaced soil layers (see Table 1), one vegetation layer, 5 snow layers (depending on the snow depth), explicit treatment of the mass of liquid water, ice and phase changes within the system of the snow and soil, runoff parameterization following the TOPMODEL concept, a tiled treatment of the sub-grid fraction of the energy and water budget balance (Dai et al. 2003) and a canopy photosynthesis-conductance mode that describes the simultaneous transfer of CO_2 and water vapor into and out of the vegetation. The model parameters include data on the global terrain, elevation, land use, vegetation, land-water mask and hybrid FAO/STATSGO soil types from the USGS, which are available at a resolution of 30 arc seconds.

Version 4.0 of the Community Land Model (CLM 4.0) (Lawrence et al. 2011; Oleson et al. 2010) is the land surface parameterization used with the Community Atmosphere Model (CAM 4.0) and the Community Climate System Model (CCSM 4.0). The CLM 4.0 includes bio-geophysics, the hydrologic cycle, biogeochemistry and the dynamic vegetation. CLM 4.0 simulates the bio-geophysical processes in each sub-grid unit independently and maintains its own prognostic variables. The parameters used in the CLM4.0 differ from those used in the CoLM. For example, the soil texture data are derived from the IGBP soil data, and the land use data are derived from the UNH Transient Land Use and Land Cover Change Dataset (http://luh.umd.edu/).

In addition to using different parameters, the two models have different structures.

For example, a model of groundwater-soil water interactions (Niu et al. 2007; Niu et al. 2005) has been incorporated into the CLM 4.0, while zero water flux at the bottom of a soil column is assumed in the CoLM. In addition, the CLM 4.0 has the same vertical discretization scheme as the CoLM (see Table 1), which makes comparing the results of the two models convenient.

3. Methods

3.1 Forecast and observation systems

Using notation similar to that used by Yilmaz et al. (2011), the forecast system can be written as

$$\mathbf{y}_{n,t}^{f} = \mathrm{M}_{n,t-1}\left(\mathbf{y}_{n,t-1}^{a}\right), \tag{1}$$

where t=1, …, T is the time index, n=1, …, N represents an ensemble member (in this study, the ensemble size is set to 100), $\mathrm{M}_{n,t-1}$ is a CoLM forced by the n-th perturbed atmospheric forcing, and $\mathbf{y}$ is a state vector containing 126 variables. The superscript "f" and "a" specify the forecast and analysis, respectively.

Let $\mathbf{x}$ be the state variables related to the water budget, that comprises of $\mathbf{SM}$ and $\mathbf{SIC}$ (the soil moisture content and the soil ice content in % at the 10 vertical levels listed in Table 1), CWC and SWE (the canopy's water content and the snow water equivalent in kg/m^2). In this study, only $\mathbf{x}$ is updated by data assimilation, while the model propagates changes to the other variables over time.

For the traditional EnKF, the forecast error covariance matrix $\mathbf{P}_t$ is obtained from the ensemble of their anomalies,

$$\mathbf{P}_t = \frac{1}{N-1}\sum_{n=1}^{N}\left(\mathbf{x}_{n,t}^{f} - \frac{1}{N}\sum_{j=1}^{N}\mathbf{x}_{j,t}^{f}\right)\left(\mathbf{x}_{n,t}^{f} - \frac{1}{N}\sum_{j=1}^{N}\mathbf{x}_{j,t}^{f}\right)^{\mathrm{T}}. \tag{2}$$

To avoid overestimation of the co-variability between shallow observations and soil

https://doi.org/10.5194/hess-2019-696
Preprint. Discussion started: 3 February 2020

moistures deeper than a threshold layer *s*, the following vertical localization function with weighting of observations $\boldsymbol{\rho}_s$ (Janjić et al. 2011) will be applied on $\mathbf{P}_t$, i.e.,

$$\boldsymbol{\rho}_s(l) = \exp\left(-\mu_s \left|d_l - d_o\right|\right) \tag{3}$$

where l represents for the l-level soil layer, d_l and d_o represent the depths of l-level soil layer and observation, respectively. $\left|d_l - d_o\right|$ is the Euclidian distance between the two layers. μ_s is estimated by minimizing the following mean square error between vertical localization function Eq (3) and a step function with threshold layer *s*,

$$M(\mu) = \sum_{l \le s}\left[\exp\left(-\mu\left|d_l - d_o\right|\right) - 1\right]^2 + \sum_{l > s}\left[\exp\left(-\mu\left|d_l - d_o\right|\right)\right]^2 \tag{4}$$

The estimated μ_s is listed in Table 2.

The observations of the soil moisture content are collected at a depth of 3 cm at 6:00 am every day (denoted by o_t). The observation system is defined as

$$o_t = \mathbf{h}\mathbf{x}_t + \varepsilon_t, \tag{5}$$

where observational operator $\mathbf{h}$ is a 22-dimensional vector which linearly interpolated the soil moisture at depths of 2.8 cm and 6.2 cm to depth of 3 cm, $\mathbf{x}_t$ represents the true values of the state variables related to the water budget at the time step t and ε_t is the observational error with mean zero and variance R_t. Since, the main objective of this study is for methodology related to linear observational operators. Choosing the linear interpolation as observational operator is only for convenience.

3.2 Assimilation with water budget constraint

Assimilating data on the soil moisture content usually results in an imbalance in

https://doi.org/10.5194/hess-2019-696
Preprint. Discussion started: 3 February 2020

the water budget. To reduce this imbalance, a weak constraint on the water budget (Yilmaz et al. 2011) is adopted in this study. The ensemble water budget residual at time step t can be expressed as

$$r_{n,t} \equiv \beta_{n,t} - \mathbf{c}^{\mathrm{T}}\mathbf{x}^{a}_{n,t}, \tag{6}$$

where

$$\beta_{n,t} = \mathbf{c}^{\mathrm{T}}\mathbf{x}^{a}_{n,t-1} + Pr_t - Ev^{f}_{n,t} - Rn^{f}_{n,t}, \tag{7}$$

where $\mathbf{c}$ is a 22-dimensional vector that converts the units to millimeters (mm) and adds up the states in $\mathbf{x}$, the diagnostic variables Pr_t, $Ev^{f}_{n,t}$ and $Rn^{f}_{n,t}$ (mm) are scalars specifying the states of the precipitation, evapotranspiration and runoff, respectively, in each pixel.

The cost function used to estimate the state variables with the weak water budget constraint (Eq. (6)) is

$$\begin{aligned} J_{n,t}(\mathbf{x}) &= \left(o_t - \mathbf{hx}\right)^{\mathrm{T}} R_t^{-1}\left(o_t - \mathbf{hx}\right) + \left(\mathbf{x} - \mathbf{x}^{f}_{n,t}\right)^{\mathrm{T}} \mathbf{P}_{s,t}^{-1}\left(\mathbf{x} - \mathbf{x}^{f}_{n,t}\right) \\ &+ \left(\beta_{n,t} - \mathbf{c}^{\mathrm{T}}\mathbf{x}\right)^{\mathrm{T}} \varphi_t^{-1}\left(\beta_{n,t} - \mathbf{c}^{\mathrm{T}}\mathbf{x}\right) \end{aligned}, \tag{8}$$

where

$$\varphi_t = \frac{1}{N-1}\sum_{n=1}^{N}\left(\beta_{n,t} - \frac{1}{N}\sum_{j=1}^{N}\beta_{j,t}\right)\times\left(\beta_{n,t} - \frac{1}{N}\sum_{j=1}^{N}\beta_{j,t}\right)^{\mathrm{T}} \tag{9}$$

is an estimate of the variance of $\beta_{n,t}$ and $\mathbf{P}_{s,t}$ represents a forecast error covariance matrix defined by

$$\mathbf{P}_{s,t} = \left[\sqrt{\boldsymbol{\lambda}_t}\right]\left[\boldsymbol{\rho}_s\right]\mathbf{P}_t\left[\boldsymbol{\rho}_s\right]\left[\sqrt{\boldsymbol{\lambda}_t}\right]. \tag{10}$$

where $\mathbf{P}_t$ is defined as Eq. (2); $\left[\boldsymbol{\rho}_s\right]$ is a diagonal matrix which localizes the soil moisture error (i.e. it is $\boldsymbol{\rho}_s$ defined by Eq. (3) for the soil moisture contents and 1 for other variables). $\left[\sqrt{\boldsymbol{\lambda}_t}\right]$ is also a diagonal matrix which inflates the forecast soil

https://doi.org/10.5194/hess-2019-696
Preprint. Discussion started: 3 February 2020

moisture error (i.e. it is a scalar λ_t for the soil moisture contents and 1 for other variable). λ_t is estimated by minimizing the -2log-likelihood of the difference between the forecast and the observation (Dee and Da Silva 1999; Liang et al. 2012; Zheng 2009),

$$-2L_{s,t}(\lambda_t) = \ln\left(\mathbf{h}\mathbf{P}_{s,t}\mathbf{h}^{\mathrm{T}} + R_t\right) + \left(o_t - \mathbf{h}\mathbf{x}_t^f\right)^{\mathrm{T}} \left(\mathbf{h}\mathbf{P}_{s,t}\mathbf{h}^{\mathrm{T}} + R_t\right)^{-1} \left(o_t - \mathbf{h}\mathbf{x}_t^f\right). \tag{11}$$

The estimated forecast error inflation factor is denoted as $\hat{\lambda}_t$. The perturbed analysis states of the variables related to water budget can be derived by minimizing Eq. (8), which has the analytic form

$$\mathbf{x}_{n,t}^a = \mathbf{x}_{n,t}^f + \mathbf{P}_t^a \mathbf{h}^{\mathrm{T}} R_t^{-1} \left(o_t + \varepsilon_{n,t} - \mathbf{h}\mathbf{x}_{n,t}^f\right) + \mathbf{P}_t^a \mathbf{c} \varphi_t^{-1} \left(\beta_{n,t} - \mathbf{c}^{\mathrm{T}} \mathbf{x}_{n,t}^f\right), \tag{12}$$

where $\varepsilon_{n,t}$ is generated from a normal distribution with mean zero and variance R_t, and its error covariance matrix is

$$\mathbf{P}_t^a = \left(\mathbf{h}^{\mathrm{T}} R_t^{-1} \mathbf{h} + \mathbf{P}_t^{-1} + \mathbf{c} \varphi_t^{-1} \mathbf{c}^{\mathrm{T}}\right)^{-1}, \tag{13}$$

For estimating the optimal threshold layer, define the -2log-likelihood of the total difference between the forecasts and the observations,

$$L_s \equiv \sum_{t=1}^{T} (-2L_{s,t}(\hat{\lambda}_t)). \tag{14}$$

The optimal threshold layer $\hat{s}$ is selected as the smallest number s such that L_s is the minimum of $\{L_2, L_3, \cdots L_{s+1}\}$. The final analysis state is the selected corresponding to the optimal threshold layer $\hat{s}$. The complete assimilation procedure is shown in Figure 2.

4. Synthetic experiments

4.1 Experimental design

https://doi.org/10.5194/hess-2019-696
Preprint. Discussion started: 3 February 2020

Hydrology and Earth System Sciences
Open Access
Discussions

To investigate the performance of the WCEnKF-based method that incorporates inflation and vertical local decomposition, synthetic experiments were performed using the CoLM. Unlike the "perfect model" assumption used in Yilmaz et al. (2011), the assumptions of this study are accounted for the error in the model, especially the structural error. Because there were structural differences in the models of the water cycle (see section 2.3) used in the two models, CLM 4.0 was used to generate the "true values" (i.e., to perform a reference run) for the synthetic experiments and CoLM was selected as the forecast operator (i.e., to perform an open-loop run). Therefore, the CLM 4.0 and the CoLM were both integrated on a 0.125° grid (see Figure 1 for the locations) with a time step of one hour. The assimilation time was set to 6:00 am every day. The assimilation experiments were conducted with 4 scenarios: a weakly constrained ensemble Kalman filter (WCEnKF), a weakly constrained ensemble Kalman filter with inflation (WCEnKF-Inf), a weakly constrained ensemble Kalman filter with inflation and localization (WCEnKF-Inf-Loc) and an ensemble Kalman filter with inflation and localization (EnKF-Inf-Loc).

Synthetic observations were obtained by interpolating $\mathbf{SM}_t$ to a depth of 3 cm and adding noise with a normal distribution ($N\left(\mu=0,\sigma=0.5\%\right)$). The initial state $\mathbf{x}_0$, was generated by running the CoLM from October 1, 2002 to June 1, 2003. Each component of the initial state was perturbed using an independent standard Gaussian random variable times 5% of magnitude of the component. The forcing data were perturbed in the manner described in Yilmaz et al. (2011). The synthetic experiments were conducted from June 1, 2003 to October 1, 2003. The state variables for each pixel were updated independently.

https://doi.org/10.5194/hess-2019-696
Preprint. Discussion started: 3 February 2020

4.2 Validation statistics

4.2.1 Model error and bias

The model errors are defined as the difference between the actual values and the model's predictions based on true initial values, and the bias is the average of the error in the model during the relevant period. Let x_t denote the true values of the soil moisture content at time *t* for a location and vertical soil layer. x_t^M denotes the model predicted soil moisture from the true state at the previous time step *t*-1. The model's bias and error variance for one step can be written as

$$b_M = \frac{1}{a_{ts}} \sum_{t=1}^{a_{ts}} \left(x_t^M - x_t \right), \tag{15}$$

$$v_M = \frac{1}{a_{ts}} \sum_{t=1}^{a_{ts}} \left(x_t^M - x_t \right)^2, \tag{16}$$

where a_{ts} is the number of time steps over which the observations made at 6:00 am each day are assimilated.

4.2.2 Validation of analysis soil moisture

The true soil moisture content values from 7:00 am to 5:00 am next day are used to validate analysis states. For a location and vertical soil layer, let $x_{t,h}$ be the true soil moisture content at hour *h* on day *t*, and $x_{t,h}^f$ represent the forecasted soil moisture content at hour *h* from analysis state x_t^a at 6:00 am on day *t*. The analysis bias is defined as

$$b_a = \frac{1}{23 a_{ts}} \sum_{t=1}^{a_{ts}} \sum_{h=7}^{29} \left(x_{t,h}^f - x_{t,h} \right). \tag{17}$$

The analysis error variance is defined as

$$\begin{aligned} v_a &= \frac{1}{23a_{ts}} \sum_{t=1}^{a_{ts}} \sum_{h=7}^{29} \left(x_{t,h}^f - x_{t,h} \right)^2 \\ &= \frac{1}{23a_{ts}} \sum_{t=1}^{a_{ts}} \sum_{h=7}^{29} \left(x_{t,h}^f - x_{t,h} - b_a \right)^2 + b_a^2 \end{aligned} . \quad (18)$$

(See Appendix A for the proof)

4.2.3 Water balance

Following Yilmaz (2011), the water budget imbalance at location is evaluated using the water balance residual,

$$R = \frac{1}{Na_{ts}} \sum_{t=1}^{a_{ts}} \sum_{n=1}^{N} r_{n,t} . \quad (19)$$

5. Real data experiments

In addition to the synthetic experiments, experiments in which the soil moisture content observed at the DGS and BTS were assimilated into the CoLM were conducted. In these experiments, the value of soil moisture was extracted from the output of the Global Land Data Assimilation (GLDAS)/CLM 2.0 model, which has been integrated continuously since 1979 (Rodell et al. 2004), and used to initialize the CoLM. Then, the model was run from October 1, 2002 to June 1, 2003. The states obtained at the end of the period were used as the initial states. In these experiments, the initial perturbation scheme, observation error variance, assimilation frequency and assimilation time were adopted from the synthetic experiments. The forcing data sets were in-situ observed; they were much more accurate than the ERA-Interim reanalysis data and were not perturbed.

In the realistic assimilation experiments, the truth is not known. Observations of the soil moisture content at hours not assimilated (7:00 am to 5:00 am next day) were used for validation. The analysis bias is estimated as

https://doi.org/10.5194/hess-2019-696
Preprint. Discussion started: 3 February 2020

Hydrology and Earth System Sciences
Discussions

$$\begin{aligned} B_a &= \frac{1}{23a_{ts}}\sum_{t=1}^{a_{ts}}\sum_{h=7}^{29}\left(\mathbf{hx}_{t,h}^{f} - o_{t,h}\right) \\ &\approx \frac{1}{23a_{ts}}\sum_{t=1}^{a_{ts}}\sum_{h=7}^{29}\left(\mathbf{h}\left(\mathbf{x}_{t,h}^{f} - \mathbf{x}_{t,h}\right)\right) \end{aligned}, \tag{20}$$

and the analysis error variance is estimated as

$$\begin{aligned} V_a &= \frac{1}{23a_{ts}}\sum_{t=1}^{a_{ts}}\sum_{h=7}^{29}\left(\mathbf{hx}_{t,h}^{f} - o_{t,h}\right)^2 \\ &\approx \frac{1}{23a_{ts}}\sum_{t=1}^{a_{ts}}\sum_{h=7}^{29}\left(\mathbf{h}\left(\mathbf{x}_{t,h}^{f} - \mathbf{x}_{t,h}\right) - B_a\right)^2 + B_a^2 + C \end{aligned} \tag{21}$$

where C is a constant which is independent of prediction schemes (See Appendix B for the proof)

Finally, the water balance residual is defined similar to Eq. (19).

6. Results

In the synthetic experiments, the magnitudes of the model's bias and error were calculated using Eqs (15) and (16), respectively, and are shown in Figure 3. It shows that the model's bias was almost negative from Figure 3a. The negative bias in the surface layer was the result of a combination of a lower surface roughness and a larger leaf area index in the CoLM; these values led to more soil evaporation and more canopy interception and could result in a smaller amount of water infiltrating the soil than the amount modeled using the CLM 4.0. In the CoLM, the porosity of each layer was less than it was in the CLM 4.0, which retained less water and contributed to the negative bias of the upper 9 layers. However, the magnitude of the bias increased to 2% in the bottom layer. The significant difference between the two models at the bottom layer could be ascribed to their different boundary conditions. Interactions between the soil moisture content and the ground water at the bottom of the soil column were modeled in the CLM 4.0 (Oleson et al. 2010) but not in the CoLM. The error in each

https://doi.org/10.5194/hess-2019-696
Preprint. Discussion started: 3 February 2020

model (Figure 3b) fluctuated in a manner similar to that of the model's bias. Unbiased observations are necessary for correcting bias in a model, which is not possible in many realistic applications, especially in assimilating remote sensing retrievals. Since satellite observations of the soil moisture content of deep layers are unavailable, only removing the bias in shallow layers would introduce error in model dynamics.

6.1 Forecast error inflation and vertical localization

In the synthetic experiments, the study domain comprised 40 pixels. Each point in the grid-scale threshold layer, the localization scale factor μ_s, was determined independently. Therefore, totally 9 sets of experiments with different localization scale factor (see Table 2) were conducted separately. Among these experiments, the "optimal" case for each pixel was defined as the case in which the column averaged analysis error (Eq. (18)) was minimized (shown in Figure 4). According to Figure 4a, the corresponding threshold layer s of μ_s was generally between 5 and 6 in both cases, which could be ascribed to the homogeneous soil texture and land cover. In the WCEnKF-Inf-Loc, there were 19 pixels in which the threshold layers were "optimal," and the layers selected in the other pixels were suboptimal (most were roughly one layer away from the "optimal" case). As shown in Figure 4b, the spatial average of the root analysis error variance (Eq. (18)) of the WCEnKF-Inf-Loc (4.09%) was comparable with the optimal value (3.84%) even though s was not selected on the basis of minimizing the analysis error.

The spatial average of the root analysis error variance in each layer in the schemes with (WCEnKF-Inf-Loc and WCEnKF-Inf) and without (WCEnKF) inflation are displayed in Figure 5a. Above 62.0 cm, the analysis errors of the schemes without inflation were substantially larger than those of the schemes with inflation for

https://doi.org/10.5194/hess-2019-696
Preprint. Discussion started: 3 February 2020

Hydrology and Earth System Sciences
Open Access
Discussions

the synthetic experiments. This suggested that inflation provided a better estimate in the layers close to observation. When no inflation was performed, the accuracy of the soil moisture content was barely improved over that of the simulation case (shown in Figure 5a).

By comparing the schemes with (WCEnKF-Inf-Loc) and without (WCEnKF-Inf) vertical localization, the impact of this approach on the assimilation accuracy in each layer is shown in Figure 5a. Because the threshold layer of the localization function $\boldsymbol{\rho}_s$ was layer 6 (36.6 cm) for 28 of the pixels (see Figure 4a), the spatial average of root analysis error variance of the results of the WCEnKF-Inf-Loc is almost identical to that of the results of the WCEnKF-Inf for depths above 36.6 cm. In contrast, inflation increased the analysis error in the soil moisture content of the deep layers in the WCEnKF-Inf. In this model, the sample error covariances of the moisture contents of shallow and deep soil were inflated by a factor greater than 6 (the average inflation factor was 6.25). This could lead to larger assimilation errors for deep soil moisture profiles in the WCEnKF-Inf. Therefore, inflation should be used with vertical localization to reduce the spurious covariance resulting from the covariance inflation-based approach.

As it was in the synthetic experiments, vertical localization (WCEnKF-Inf-Loc) was helpful in avoiding erroneous estimates of the soil moisture contents at lower levels (in the WCEnKF-Inf). A comparison of the analysis error at a depth of 3 cm (i.e., the depth of the assimilated observations was 3 cm) in the models with (WCEnKF-Inf and WCEnKF-Inf-Loc) and without (WCEnKF) inflation showed that the inflation technique significantly reduces the analysis error at the depth at which observations are made.

In the real data experiments, the spatial averages of root analysis error variance

https://doi.org/10.5194/hess-2019-696
Preprint. Discussion started: 3 February 2020

in each layer (Eq. (21)) are shown in Figures 6a and 7a. To validate the effect of the vertical localization, the results of the "optimal" (based on the minimum analysis error at the four observation sites) and WCEnKF-Inf-Loc were compared. In the experiments using the data from the DGS, the threshold, *s*, was set to layer 2 (2.8 cm) for the "optimal" case and layer 5 (21.2 cm) for the WCEnKF-Inf-Loc. However, the analysis error in the two models at each layer in which observations were made remained comparable. In the experiments using the data from the BTS, the value of *s* was set to 3 (6.2 cm) in both models, which resulted in equivalent analysis errors.

Unlike the truth at all model depths are available in the synthetic experiments, the observations only available at the four depths for the two stations, which did not cover the all model layers. Therefore, the analysis error in layers deeper than the observation could not be checked.

6.2 The water budget constraint

In the synthetic experiment, the weak constraint on the water budget reduced the water balance residual significantly in each pixel and the results are shown in Figure 8. It shows that, the water balance residuals for the assimilation scheme with water budget constraint are smaller than those without water budget constraint. The forecast error covariance matrix inflation can lead to the increase of water balance residual, while the vertical localization technique (i.e. WCEnKF-Inf-Loc scheme) can restrict it in a rational range. In the WCEnKF-Inf-Loc, the spatial average of the water balance residual was 0.0742 mm, which was much less than that of the EnKF-Inf-Loc (0.2259 mm). The spread of the water balance residual was also smaller in the WCEnKF-Inf-Loc, which signals a more stable water balance budget. Therefore, the weak constraint on the water budget resulted in an assimilation accuracy that was

https://doi.org/10.5194/hess-2019-696
Preprint. Discussion started: 3 February 2020

Hydrology and Earth System Sciences Discussions

comparable to that of unconstrained filters but had a much smaller water budget residual, which is consistent with the results of previous studies (Yilmaz et al. 2011; Yilmaz et al. 2012).

To investigate the role of the water budget constraint in the assimilation process in the synthetic experiment, the spatial averaged root analysis error variance (Eq. (18)) of the schemes with (WCEnKF-Inf-Loc) and without (EnKF-Inf-Loc) the water budget constraint were compared. In the EnKF-Inf-Loc, the threshold layers were adopted from the WCEnKF-Inf-Loc. According to Figure 5a, the spatial averaged root analysis error variances of the two models were almost identical (1.83% for the WCEnKF-Inf-Loc and 2.00% for the EnKF-Inf-Loc) in the layers that were shallower than 21.2 cm. However, for the layers that were deeper than 36.6 cm, the average RSME of the EnKF-Inf-Loc (4.95%) was less than that of the WCEnKF-Inf-Loc (5.87%). This could be the compensation for the reduction in the water balance residual.

In the real data experiments, consistent reductions in the water budget residual were obtained from the different experiments. The water balance residuals (Eq. (19)) in the EnKF-Inf-Loc at the DGS and BTS were 0.1545 mm and 0.1792 mm, respectively. In contrast, the residuals were reduced to 0.0386 mm and 0.0131 mm, respectively, at the two stations in the WCEnKF-Inf-Loc, which supports the robustness of the weak constraint on the water budget.

7. Discussion

7.1 Covariance inflation and vertical localization

In this study, the cost function used to estimate the state variables with the weak water budget constraint (Eq. (8)) consists of three parts, which are related with

https://doi.org/10.5194/hess-2019-696
Preprint. Discussion started: 3 February 2020

observations, model forecasts and water residual (Yilmaz et al. 2012). It is represented as a summation of three scalars, no matter how many observations are assimilated. Therefore, inflating of one scalar (e.g., model forecasts) seems to have the similar impact as deflating another one (e.g., water residual), particularly the weights associated in this problem can be shown as function of the ratio of these three scalars. Specifically, inflation of forecast error covariance has somewhat similar impact with deflation the water balance residual covariance. Accordingly, it is plain obvious that the water balance residual of the scheme WCEnKF-Inf is larger than that of the scheme WCEnKF.According to Figures 5a-7a, the covariance inflation improved the estimates of the soil moisture content in the shallow layers independently of whether vertical localization was used. This is primarily because the observation operator, **h**, is the linear operator that was used to interpolate the soil moisture content at depths of 2.8 cm and 6.2 cm to a depth of 3 cm. Then, the likelihood function for the inflation factor (Eq. (11)) depends only on the observations and predictions of the soil moisture content in the 2nd and 3rd layers. The mean value of the inflation factor is 6.25 for WCEnKF-Inf, indicating that the initial forecast spread is not large enough. This leads to an improvement in the forecast error statistics in the shallow layers, and to further improvements in the soil moisture contents of those layers. However, the soil moisture contents of the deep layers are not directly related to the inflation factor. Inflating the forecast errors in the deep layers leads to an overestimation of the corresponding forecast error covariance, and could lead to larger analysis errors in the deep layers (see WCEnKF-Inf in Figure 5a). Therefore in this study, the vertical localization approach was developed to prevent soil moisture over fitting for deep layers. Using all observations for shreshould *s* is only for model selection (from the 10 layers), not for fitting parameter.When vertical localization is used, the soil moisture contents of the

https://doi.org/10.5194/hess-2019-696
Preprint. Discussion started: 3 February 2020

Hydrology and Earth System Sciences Open Access Discussions EGU

deep layers are not significantly updated. Consequently, larger errors are avoided in the deep layers (see WCEnKF-Inf-Loc in Figure 5a).

Comparing to traditional EnKF without inflation and localization, although mainly the soil moisture contents of layers above the threshold layer (usually the 5th or 6th layer) were updated at each time step during the assimilation process when the WCEnKF-Inf-Loc was used, Figure 5a shows that the soil moisture contents of the layers below the threshold layer, especially the 6th and 7th layers, are also improved. This may be because the model propagates changes in the shallow layers downward, adjusting the soil moisture contents of the deep layers. Because the soil moisture content of layers above the threshold layer was improved during the previous time step, this process results in better predictions of the soil moisture contents of layers below the threshold layer, and therefore, reduces the analysis error in layers below the threshold layer.

7.2 Bias correction

Geophysical models are never perfect and usually produce estimates with biases that vary in time and in space (Reichle 2008). Therefore bias correction is important for assimilating data into models. The model bias can be removed when all model variables are observed, such as the case studied by Yilmaz et al (2011). However in this study only soil moisture in shallow layers can be observed (in order to mimic the satellite observation). There is no observation available to correct the bias of soil moistures in deeper layers. If only remove the bias in shallow layers, it would introduce error in model dynamics. Therefore in this study, we still use traditional (bias-blind) data assimilation framework.

However in the present study, the analysis error variance was decomposed to a short-lived component (Figures 5b-7b) and a bias component (Figures 5c-7c) for the synthetic experiment and the two real data experiments, respectively. It shows that for our proposed bias-blind data assimilation scheme (WCEnKF-Inf-Loc), both short-lived errors and biases reduce in the layers close to observation, while maintain the similar levels for the deeper layers. The covariance inflation can play an important role in bias reduction. Bias can only be seen during whole assimilation period. At an instant time, bias and error are mixed. For the traditional EnKF, the forecast error covariance matrix obtained from the ensemble of their anomalies (Eq. (2)) mainly represents short-lived error, so it has to be inflated to include error related to bias.

There are other bias estimation approaches in data assimilation. For example, treading bias as model variables and estimate in assimilation (De Lannoy et al. 2007; Dee and Da Silva 1997; Dee and Da Silva 1998), adjusting the state variable of the forecast model not only their covariance matrix in each forecast step (Zhang et al. 2015; Zhang et al. 2014), addressing the biases in the model and observations by rescaling their cumulative distribution functions (Koster et al. 2009; Reichle and Koster 2004). The scheme proposed here can provide a base line to validate the efficacy of these approaches and could be further improved after these bias corrections.

8. Conclusions

In this study, observations of the soil moisture content at a depth of 3 cm were assimilated using an ensemble Kalman filter with three improvements. Firstly, an adaptive forecast error inflation based on maximum-likelihood estimation was adopted to reduce the analysis error. This study supports the idea that the proper form of the forecast error covariance matrix is crucial for reducing the analysis error near

https://doi.org/10.5194/hess-2019-696
Preprint. Discussion started: 3 February 2020

Hydrology and Earth System Sciences
Open Access
Discussions

the layers in which observations are made. Secondly, an adequate vertical localization for the ensemble-based filter was proposed associated with the forecast error covariance inflation, to avoid misestimates of the soil moisture contents of deep layers. Lastly, a constraint on the water balance was used in this study to reduce the water budget residual substantially without significantly changing the assimilation accuracy. The experiment results of synthetic study and real data show that the WCEnKF-Inf-Loc assimilation scheme can reduce both the short-lived analysis error and the analysis bias in the shallow layers, which also lead to a rational water budget residual.

The work presented in this paper may have some limitations. For example, the iterations involved in the optimization process reduce the computational efficiency, and the study area was homogeneous grassland without a compound type of land cover. Because the accuracy of the microwave soil moisture content is significantly affected by the land cover type (Dorigo et al. 2010), it is necessary to perform more experiments using other regions.

In the near future, we plan to validate the major conclusions under different soil conditions and land cover types. Vertical localization, which uses adjacent observations, should also be tested in future work. More detailed analyses of the bias correction for assimilating remote sensing retrievals should be performed. The response of the analytic soil moisture content to weather predictions also needs to be investigated. Completing these studies should improve the state of research into land-atmosphere interactions.

https://doi.org/10.5194/hess-2019-696
Preprint. Discussion started: 3 February 2020

Data availability The soil moisture observation and hourly measurements of forcing data are available at http://www.ceop.net. The ERA-interim forcing data used in the synthetic experiments is obtained from https://apps.ecmwf.int/datasets. The downward shortwave and longwave radiation data used in the realistic experiments are provided by the Japanese Meteorological Agency at https://www.jma.go.jp/en.

Author Contributions BD performed the simulations and assimilations. XZ designed the research. GW analyzed the results. TL collected and preprocessed the data. GW and XZ prepared the manuscript with contributions from all co-authors.

Conflicts of Interest The authors declare that they have no conflict of interest.

Acknowledgement This study was funded by the National Basic Research Program of China (2015CB953703), the National Key R&D Program of China (2017YFA0603601) and the National Natural Science Foundation of China (41405098 and 41705086). We would like to thank the Editor and three anonymous reviewers for their insightful comments in improving the manuscript. We also thank Drs. Yongjiu Dai and Qingyun Duan for their help in land surface model.

Appendix A. Proof of Eq. (18)

For a location and vertical soil layer, the analysis error variance in the synthetic experiment is defined as

https://doi.org/10.5194/hess-2019-696
Preprint. Discussion started: 3 February 2020

Hydrology and Earth System Sciences Discussions
Open Access

$$\begin{aligned}
v_a &= \frac{1}{23a_{ts}}\sum_{t=1}^{a_{ts}}\sum_{h=7}^{29}\left(x_{t,h}^{f}-x_{t,h}\right)^2 \\
&= \frac{1}{23a_{ts}}\sum_{t=1}^{a_{ts}}\sum_{h=7}^{29}\left(x_{t,h}^{f}-x_{t,h}-b_a+b_a\right)^2 \\
&= \frac{1}{23a_{ts}}\sum_{t=1}^{a_{ts}}\sum_{h=7}^{29}\left(x_{t,h}^{f}-x_{t,h}-b_a\right)^2+b_a^2+\frac{2b_a}{23a_{ts}}\sum_{t=1}^{a_{ts}}\sum_{h=7}^{29}\left(x_{t,h}^{f}-x_{t,h}-b_a\right)
\end{aligned} \tag{A1}$$

From the definition of analysis bias (Eq. (17)), the last term on the right hand side of is zero, so Eq. (18) is proved.

Appendix B. Proof of Eqs. (20)-(21)

Since

$$\begin{aligned}
B_a &= \frac{1}{23a_{ts}}\sum_{t=1}^{a_{ts}}\sum_{h=7}^{29}\left(\mathbf{hx}_{t,h}^{f}-o_{t,h}\right) \\
&= \frac{1}{23a_{ts}}\sum_{t=1}^{a_{ts}}\sum_{h=7}^{29}\left(\mathbf{hx}_{t,h}^{f}-\mathbf{h}x_{t,h}-\varepsilon_{t,h}\right) \\
&= \frac{1}{23a_{ts}}\sum_{t=1}^{a_{ts}}\sum_{h=7}^{29}\left(\mathbf{h}\left(\mathbf{x}_{t,h}^{f}-\mathbf{x}_{t,h}\right)\right)-\frac{1}{23a_{ts}}\sum_{t=1}^{a_{ts}}\sum_{h=7}^{29}\varepsilon_{t,h}
\end{aligned} \tag{B1}$$

The second term of the right-hand side of Eq. (B1) is approximate zero, because the observation error $\varepsilon_{t,h}$ has zero mean. Therefore Eq. (20) holds.

Since

$$\begin{aligned}
V_a &= \frac{1}{23a_{ts}}\sum_{t=1}^{a_{ts}}\sum_{h=7}^{29}\left(\mathbf{hx}_{t,h}^{f}-o_{t,h}\right)^2 \\
&= \frac{1}{23a_{ts}}\sum_{t=1}^{a_{ts}}\sum_{h=7}^{29}\left(\mathbf{hx}_{t,h}^{f}-\left(\mathbf{h}x_{t,h}+\varepsilon_{t,h}\right)-B_a+B_a\right)^2 \\
&= \frac{1}{23a_{ts}}\sum_{t=1}^{a_{ts}}\sum_{h=7}^{29}\left(\mathbf{h}\left(\mathbf{x}_{t,h}^{f}-x_{t,h}\right)-B_a\right)^2+B_a^2+\frac{1}{23a_{ts}}\sum_{t=1}^{a_{ts}}\sum_{h=7}^{29}\varepsilon_{t,h}^2 \\
&+\frac{1}{23a_{ts}}\sum_{t=1}^{a_{ts}}\sum_{h=7}^{29}\left(\mathbf{h}\left(\mathbf{x}_{t,h}^{f}-x_{t,h}\right)-B_a\right)B_a \\
&+\frac{1}{23a_{ts}}\sum_{t=1}^{a_{ts}}\sum_{h=7}^{29}\left[\mathbf{h}\left(\mathbf{x}_{t,h}^{f}-x_{t,h}\right)-B_a\right]\varepsilon_{t,h}+\frac{B_a}{23a_{ts}}\sum_{t=1}^{a_{ts}}\sum_{h=7}^{29}\varepsilon_{t,h}
\end{aligned} \tag{B2}$$

https://doi.org/10.5194/hess-2019-696
Preprint. Discussion started: 3 February 2020

Hydrology and Earth System Sciences Discussions

The third term of the right-hand side Eq. (B2) is denoted as C, it is determined by all the true values and observations, but not related to any prediction scheme. By the definition of analysis bias B_a (Eq. 20), the fourth term of the right-hand side Eq. (B1) is approximate zero; since the observation error $\varepsilon_{t,h}$ has zero mean and is statistically independent of the forecast error $\mathbf{h}\left(\mathbf{x}_{t,h}^{f} - x_{t,h}\right)$, the fifth and sixth terms of the right-hand side Eq. (B1) are approximate zero too. Therefore, Eq. (21) holds.

https://doi.org/10.5194/hess-2019-696
Preprint. Discussion started: 3 February 2020

References

Anderson, J.L. and Anderson, S.L., 1999. A Monte Carlo implementation of the nonlinear fltering problem to produce ensemble assimilations and forecasts. Monthly Weather Review, 127: 2741-2758.

Bartalis, Z., Wagner, W., Naeimi, V., Hasenauer, S., Scipal, K., Bonekamp, H., Figa, J. and Anderson, C., 2007. Initial soil moisture retrievals from the METOP-A Advanced Scatterometer (ASCAT). Geophysical Research Letters, 34(20).

Bauser, H.H., Berg, D., Klein, O. and Roth, K., 2018. Inflation method for ensemble Kalman filter in soil hydrology. Hydrology and Earth System Sciences, 22(9): 4921-4934.

Bonan, G.B., 1996. Land surface model (LSM version 1.0) for ecological, hydrological, and atmospheric studies: Technical description and users guide. Technical note, National Center for Atmospheric Research, Boulder, CO (United States). Climate and Global Dynamics Div.

Bosilovich, M.G. and Lawford, R., 2002. Coordinated enhanced observing period (CEOP) international workshop. Bulletin of the American Meteorological Society, 83(10): 1495-1499.

Chen, F., Crow, W.T. and Ryu, D., 2014. Dual Forcing and State Correction via Soil Moisture Assimilation for Improved Rainfall-Runoff Modeling. Journal of Hydrometeorology, 15(5): 1832-1848.

Constantinescu, E.M., Sandu, A., Chai, T. and Carmichael, G.R., 2007. Ensemble-based chemical data assimilation I: general approach. Quarterly Journal of the Royal Meteorological Society, 133: 1229-1243.

Crow, W.T., Chen, F., Reichle, R.H. and Liu, Q., 2017. L band microwave remote sensing and land data assimilation improve the representation of prestorm soil moisture conditions for hydrologic forecasting. Geophysical Research Letters, 44(11): 5495-5503.

Crow, W.T. and Loon, E.V., 2006. Impact of incorrect model error assumptions on the sequential assimilation of remotely sensed surface soil moisture. Journal of Hydrometeorology, 7: 421-432.

Crow, W.T. and Wood, E.F., 2003. The assimilation of remotely sensed soil brightness temperature imagery into a land surface model using Ensemble Kalman filtering: a case study based on ESTAR measurements during SGP97. Advances in Water Resources, 26: 137-149.

Dai, Y., Zeng, X., Dickinson, R.E., Baker, I., Bonan, G.B., Bosilovich, M.G., Denning, A.S., Dirmeyer, P.A., Houser, P.R., Niu, G., Oleson, K.W., Schlosser, C.A. and Yang, Z.-L., 2003. The Common Land Model. Bulletin of the American Meteorological Society, 84(8): 1013-1023.

De Lannoy, G.J.M. and Reichle, R.H., 2016. Global Assimilation of Multiangle and Multipolarization SMOS Brightness Temperature Observations into the GEOS-5 Catchment Land Surface Model for Soil Moisture Estimation. Journal of Hydrometeorology, 17(2): 669-691.

De Lannoy, G.J.M., Reichle, R.H., Houser, P.R., Pauwels, V.R.N. and Verhoest, N.E.C., 2007. Correcting for forecast bias in soil moisture assimilation with the ensemble Kalman filter. Water Resources Research, 43(9): n/a-n/a.

Dee, D.P. and Da Silva, A.M., 1997. Data assimilation in the presence of forecast bias. Quart. J. Roy. Meteor. Soc., accepted.

Dee, D.P. and Da Silva, A.M., 1998. Data assimilation in the presence of forecast bias. Quarterly Journal of the Royal Meteorological Society, 124(545): 269-295.

Dee, D.P. and Da Silva, A.M., 1999. Maximum-likelihood estimation of forecast and

https://doi.org/10.5194/hess-2019-696
Preprint. Discussion started: 3 February 2020

observation error covariance parameters. Part I: Methodology. Monthly Weather Review, 127(8): 1822-1834.

Dee, D.P., Gaspari, G., Redder, C., Rukhovets, L. and Da Silva, A.M., 1999. Maximum-likelihood estimation of forecast and observation error covariance parameters. Part II: Applications. Monthly weather review, 127(8): 1835-1849.

Dee, D.P., Uppala, S.M., Simmons, A.J., Berrisford, P., Poli, P., Kobayashi, S., Andrae, U., Balmaseda, M.A., Balsamo, G., Bauer, P., Bechtold, P., Beljaars, A.C.M., van de Berg, L., Bidlot, J., Bormann, N., Delsol, C., Dragani, R., Fuentes, M., Geer, A.J., Haimberger, L., Healy, S.B., Hersbach, H., Hólm, E.V., Isaksen, L., Kållberg, P., Köhler, M., Matricardi, M., McNally, A.P., Monge-Sanz, B.M., Morcrette, J.J., Park, B.K., Peubey, C., de Rosnay, P., Tavolato, C., Thépaut, J.N. and Vitart, F., 2011. The ERA-Interim reanalysis: configuration and performance of the data assimilation system. Quarterly Journal of the Royal Meteorological Society, 137(656): 553-597.

Delworth, T.L. and Manabe, S., 1988. The influence of potential evaporation on the variabilities of simulated soil wetness and climate. Journal of Climate, 1(5): 523-547.

Dickinson, R.E., Henderson-Sellers, A. and Kennedy, P.J., 1993. Biosphere Atmosphere Transfer Scheme (BATS) Version le as Coupled to the NCAR Community Climate Model.

Dorigo, W.A., Scipal, K., Parinussa, R.M., Liu, Y.Y., Wagner, W., de Jeu, R.A.M. and Naeimi, V., 2010. Error characterisation of global active and passive microwave soil moisture datasets. Hydrology and Earth System Sciences, 14(12): 2605-2616.

Dorigo, W.A., Wagner, W., Hohensinn, R., Hahn, S., Paulik, C., Xaver, A., Gruber, A., Drusch, M., Mecklenburg, S., van Oevelen, P., Robock, A. and Jackson, T., 2011. The International Soil Moisture Network: a data hosting facility for global in situ soil moisture measurements. Hydrology and Earth System Sciences, 15(5): 1675-1698.

Dumedah, G. and Walker, J.P., 2014. Evaluation of Model Parameter Convergence when Using Data Assimilation for Soil Moisture Estimation. Journal of Hydrometeorology, 15(1): 359-375.

El Gharamti, M., Raeder, K., Anderson, J. and Wang, X.G., 2019. Comparing Adaptive Prior and Posterior Inflation for Ensemble Filters Using an Atmospheric General Circulation Model. Monthly Weather Review, 147(7): 2535-2553.

Entekhabi, D., Njoku, E.G., O'Neill, P.E., Kellogg, K.H., Crow, W.T., Edelstein, W.N., Entin, J.K., Goodman, S.D., Jackson, T.J. and Johnson, J., 2010. The soil moisture active passive (SMAP) mission. Proceedings of the IEEE, 98(5): 704-716.

Evensen, G., 1994. Sequential data assimilation with a nonlinear quasi-geostrophic model using Monte Carlo methods to forecast error statistics. Journal of Geophysical Research, 99: 10143-10162.

Gruber, A., Crow, W.T. and Dorigo, W.A., 2018. Assimilation of Spatially Sparse In Situ Soil Moisture Networks into a Continuous Model Domain. Water Resources Research, 54(2): 1353-1367.

GUSEV, Y. and Novak, V., 2007. Soil water–main water resources for terrestrial ecosystems of the biosphere. J. Hydrol. Hydromech, 55(1): 3-15.

Han, E., Crow, W.T., Holmes, T. and Bolten, J., 2014. Benchmarking a Soil Moisture Data Assimilation System for Agricultural Drought Monitoring. Journal of

https://doi.org/10.5194/hess-2019-696
Preprint. Discussion started: 3 February 2020

Hydrology and Earth System Sciences
Open Access
Discussions

Hydrometeorology, 15(3): 1117-1134.

Huang, C., Li, X. and Lu, L., 2008. Retrieving soil temperature profile by assimilating MODIS LST products with ensemble Kalman filter. Remote Sensing of Environment, 112(4): 1320-1336.

Janjić, T., Nerger, L., Albertella, A., Schröter, J. and Skachko, S., 2011. On Domain Localization in Ensemble-Based Kalman Filter Algorithms. Monthly Weather Review, 139(7): 2046-2060.

Kerr, Y.H., Waldteufel, P., Wigneron, J.-P., Delwart, S., Cabot, F., Boutin, J., Escorihuela, M.-J., Font, J., Reul, N. and Gruhier, C., 2010. The SMOS mission: New tool for monitoring key elements ofthe global water cycle. Proceedings of the IEEE, 98(5): 666-687.

Koster, R.D., Guo, Z.C., Yang, R.Q., Dirmeyer, P.A., Mitchell, K. and Puma, M.J., 2009. On the Nature of Soil Moisture in Land Surface Models. Journal of Climate, 22(16): 4322-4335.

Kumar, S.V., Peters-Lidard, C.D., Mocko, D., Reichle, R., Liu, Y.Q., Arsenault, K.R., Xia, Y.L., Ek, M., Riggs, G., Livneh, B. and Cosh, M., 2014. Assimilation of Remotely Sensed Soil Moisture and Snow Depth Retrievals for Drought Estimation. Journal of Hydrometeorology, 15(6): 2446-2469.

Lawford, R., Stewart, R., Roads, J., Isemer, H., Manton, M., Marengo, J., Yasunari, T., Benedict, S., Koike, T. and Williams, S., 2004. Advancing global-and continental-scale hydrometeorology: Contributions of GEWEX hydrometeorology panel. Bulletin of the American Meteorological Society, 85(12): 1917-1930.

Lawrence, D.M., Oleson, K.W., Flanner, M.G., Thornton, P.E., Swenson, S.C., Lawrence, P.J., Zeng, X., Yang, Z.-L., Levis, S., Sakaguchi, K., Bonan, G.B.

and Slater, A.G., 2011. Parameterization improvements and functional and structural advances in Version 4 of the Community Land Model. Journal of Advances in Modeling Earth Systems, 3(3).

Li, B., Toll, D., Zhan, X. and Cosgrove, B., 2012. Improving estimated soil moisture fields through assimilation of AMSR-E soil moisture retrievals with an ensemble Kalman filter and a mass conservation constraint. Hydrology and Earth System Sciences, 16(1): 105-119.

Liang, X., Zheng, X., Zhang, S., Wu, G., Dai, Y. and Li, Y., 2012. Maximum likelihood estimation of inflation factors on error covariance matrices for ensemble Kalman filter assimilation. Quarterly Journal of the Royal Meteorological Society, 138: 263-273.

Loizu, J., Massari, C., Alvarez-Mozos, J., Tarpanelli, A., Brocca, L. and Casali, J., 2018. On the assimilation set-up of ASCAT soil moisture data for improving streamflow catchment simulation. Advances in Water Resources, 111: 86-104.

Lu, H., Koike, T., Yang, K., Hu, Z.Y., Xu, X.D., Rasmy, M., Kuria, D. and Tamagawa, K., 2012. Improving land surface soil moisture and energy flux simulations over the Tibetan plateau by the assimilation of the microwave remote sensing data and the GCM output into a land surface model. International Journal of Applied Earth Observation and Geoinformation, 17: 43-54.

Lu, H., Yang, K., Koike, T., Zhao, L. and Qin, J., 2015. An Improvement of the Radiative Transfer Model Component of a Land Data Assimilation System and Its Validation on Different Land Characteristics. Remote Sensing, 7(5): 6358-6379.

McColl, K.A., He, Q., Lu, H. and Entekhabi, D., 2019. Short-Term and Long-Term Surface Soil Moisture Memory Time Scales Are Spatially Anticorrelated at

https://doi.org/10.5194/hess-2019-696
Preprint. Discussion started: 3 February 2020

Global Scales. Journal of Hydrometeorology, 20(6): 1165-1182.

Miyoshi, T., 2011. The Gaussian approach to adaptive covariance inflation and its implementation with the local ensemble transform Kalman filter. Monthly Weather Review, 139: 1519-1534.

Miyoshi, T., Kalnay, E. and Li, H., 2012. Estimating and including observation-error correlations in data assimilation. Inverse Problems in Science & Engineering, 32: 1-12.

Niu, G.-Y., Yang, Z.-L., Dickinson, R.E., Gulden, L.E. and Su, H., 2007. Development of a simple groundwater model for use in climate models and evaluation with Gravity Recovery and Climate Experiment data. Journal of Geophysical Research, 112(D7).

Niu, G.Y., Yang, Z.L., Dickinson, R.E. and Gulden, L.E., 2005. A simple TOPMODEL‐based runoff parameterization (SIMTOP) for use in global climate models. Journal of Geophysical Research: Atmospheres (1984–2012), 110(D21).

Njoku, E.G., Jackson, T.J., Lakshmi, V., Chan, T.K. and Nghiem, S.V., 2003. Soil moisture retrieval from AMSR-E. Geoscience and Remote Sensing, IEEE Transactions on, 41(2): 215-229.

Oleson, K.W., Lawrence, D.M., Gordon, B., Flanner, M.G., Kluzek, E., Peter, J., Levis, S., Swenson, S.C., Thornton, E. and Feddema, J., 2010. Technical description of version 4.0 of the Community Land Model (CLM).

Pan, M. and Wood, E.F., 2006. Data assimilation for estimating the terrestrial water budget using a constrained ensemble Kalman filter. Journal of Hydrometeorology, 7(3): 534-547.

Pielke, R.A., 2001. Influence of the spatial distribution of vegetation and soils on the

https://doi.org/10.5194/hess-2019-696
Preprint. Discussion started: 3 February 2020

prediction of cumulus Convective rainfall. Reviews of Geophysics, 39(2): 151-177.

Pinnington, E., Quaife, T. and Black, E., 2018. Impact of remotely sensed soil moisture and precipitation on soil moisture prediction in a data assimilation system with the JULES land surface model. Hydrology and Earth System Sciences, 22(4): 2575-2588.

Raanes, P.N., Bocquet, M. and Carrassi, A., 2019. Adaptive covariance inflation in the ensemble Kalman filter by Gaussian scale mixtures. Quarterly Journal of the Royal Meteorological Society, 145(718): 53-75.

Reichle, R.H., 2008. Data assimilation methods in the Earth sciences. Advances in Water Resources, 31: 1411-1418.

Reichle, R.H., De Lannoy, G.J.M., Liu, Q., Koster, R.D., Kimball, J.S., Crow, W.T., Ardizzone, J.V., Chakraborty, P., Collins, D.W., Conaty, A.L., Girotto, M., Jones, L.A., Kolassa, J., Lievens, H., Lucchesi, R.A. and Smith, E.B., 2017. Global Assessment of the SMAP Level-4 Surface and Root-Zone Soil Moisture Product Using Assimilation Diagnostics. Journal of Hydrometeorology, 18(12): 3217-3237.

Reichle, R.H. and Koster, R.D., 2004. Bias reduction in short records of satellite soil moisture. Geophysical Research Letters, 31(L19501).

Reichle, R.H. and Koster, R.D., 2005. Global assimilation of satellite surface soil moisture retrievals into the NASA Catchment land surface model. Geophysical Reasearch Letters, 32.

Robock, A., Vinnikov, K.Y., Srinivasan, G., Entin, J.K., Hollinger, S.E., Speranskaya, N.A., Liu, S. and Namkhai, A., 2000. The global soil moisture data bank. Bulletin of the American Meteorological Society, 81(6): 1281-1299.

https://doi.org/10.5194/hess-2019-696
Preprint. Discussion started: 3 February 2020

Hydrology and Earth System Sciences
Open Access
EGU
Discussions

Rodell, M., Houser, P.R., Jambor, U., Gottschalck, J., Mitchell, K., Meng, C.J., Arsenault, K., Cosgrove, B., Radakovich, J., Bosilovich, M., Entin*, J.K., Walker, J.P., Lohmann, D. and Toll, D., 2004. The Global Land Data Assimilation System. Bulletin of the American Meteorological Society, 85(3): 381-394.

Santanello, J.A., Kumar, S.V., Peters-Lidard, C.D. and Lawston, P.M., 2016. Impact of Soil Moisture Assimilation on Land Surface Model Spinup and Coupled Land-Atmosphere Prediction. Journal of Hydrometeorology, 17(2): 517-540.

Wang, X. and Bishop, C.H., 2003. A comparison of breeding and ensemble transform kalman filter ensemble forecast schemes. Journal of the Atmospheric Sciences, 60: 1140-1158.

Wei, J., Dirmeyer, P.A., Guo, Z., Zhang, L. and Misra, V., 2010. How Much Do Different Land Models Matter for Climate Simulation? Part I: Climatology and Variability. Journal of Climate, 23(11): 3120-3134.

Wu, G., Zheng, X., Wang, L., Zhang, S., Liang, X. and Li, Y., 2013. A New Structure for Error Covariance Matrices and Their Adaptive Estimation in EnKF Assimilation. Quarterly Journal of the Royal Meteorological Society, 139: 795-804.

Yang, K., Koike, T., Kaihotsu, I. and Qin, J., 2009. Validation of a dual-pass microwave land data assimilation system for estimating surface soil moisture in semiarid regions. Journal of Hydrometeorology, 10: 780-793.

Yang, K., Zhu, L., Zhao, Y.C.L., Qin, J., Lu, H., Tang, W., Han, M., Ding, B. and Fang, N., 2016. Land surface model calibration through microwave data assimilation for improving soil moisture simulations. Journal of Hydrology, 533: 266-276.

Yang, S.-C., Kalnay, E. and Enomoto, T., 2015. Ensemble singular vectors and their

https://doi.org/10.5194/hess-2019-696
Preprint. Discussion started: 3 February 2020

Hydrology and Earth System Sciences
Open Access
Discussions

use as additive inflation in EnKF. Tellus A, 67.

Yilmaz, M.T., DelSole, T. and Houser, P.R., 2011. Improving Land Data Assimilation Performance with a Water Budget Constraint. Journal of Hydrometeorology, 12(5): 1040-1055.

Yilmaz, M.T., DelSole, T. and Houser, P.R., 2012. Reducing Water Imbalance in Land Data Assimilation: Ensemble Filtering without Perturbed Observations. Journal of Hydrometeorology, 13(1): 413-420.

Zhang, S., Chen, X.Z.J., Chen, Z., Dan, B., Yi, X., Wang, L. and Wu, G., 2015. A global carbon assimilation system using a modified ensemble Kalman filter. Geoscientific Model Development, 8: 805-816.

Zhang, S., Yi, X., Zheng, X., Chen, Z., Dan, B. and Zhang, X., 2014. Global carbon assimilation system using a local ensemble Kalman filter with multiple ecosystem models. Journal of Geophysical Research-Biogeosciences, 119(11): 2171-2187.

Zhao, L. and Yang, Z.L., 2018. Multi-sensor land data assimilation: Toward a robust global soil moisture and snow estimation. Remote Sensing of Environment, 216: 13-27.

Zheng, X., 2009. An adaptive estimation of forecast error covariance parameters for Kalman filtering data assimilation. Advances in Atmospheric Sciences, 26(1): 154-160.

Figure captions

Figure 1. The topography and river distribution (left plot) and the geographical location of the synthetic study area and the two application stations, the DGS and the BTS (right plot).

Figure 2. The assimilation procedure and localization scale factor estimation in the experiments. All of the equations are in accordance with that described in the text.

Figure 3. The areal average of the model's bias (a) and error (b) for one step in the soil moisture content between the CoLM and the CLM 4.0. The horizontal axis represents the layer depth.

Figure 4. The threshold layers and analysis error for each pixel in the synthetic experiment. Graph (a) illustrates the optimal and WCEnKF-Inf-Loc threshold layers of each pixel. Graph (b) shows the column RSME of each pixel in different schemes with water balance constraint (Optimal, WCEnKF-Inf-Loc, WCEnKF-Inf and WCEnKF). The horizontal axes of (a) and (b) represent the 40 pixels in the study domain.

Figure 5. The assimilation results in each layer for an ensemble Kalman filter with forecast error inflation and vertical localization (EnKF-Inf-Loc), a weakly constrained ensemble Kalman filter with forecast error inflation and vertical localization (WCEnKF-Inf-Loc), a weakly constrained ensemble Kalman filter with forecast error inflation (WCEnKF-Inf), a weakly constrained ensemble Kalman filter (WCEnKF), traditional assimilation (EnKF) and an open-loop simulation. Graphic (a) is for spatial

https://doi.org/10.5194/hess-2019-696
Preprint. Discussion started: 3 February 2020

Hydrology and Earth System Sciences Discussions

averaged analysis error of the soil moisture content, (b) is for the short-lived error and (c) is for the analysis bias.

Figure 6. The assimilation results in each observation layer for an ensemble Kalman filter with forecast error inflation and vertical localization (EnKF-Inf-Loc), a weakly constrained ensemble Kalman filter with forecast error inflation and vertical localization (WCEnKF-Inf-Loc), a weakly constrained ensemble Kalman filter with forecast error inflation (WCEnKF-Inf), a weakly constrained ensemble Kalman filter (WCEnKF), traditional assimilation (EnKF) and an open-loop simulation. Graphic (a) is for spatial averaged analysis error of the soil moisture content, (b) is for the short-lived error and (c) is for the analysis bias.

Figure 7. Same as Figure 6, but for BTS station.

Figure 8. The box plot of the water balance residual in all 40 pixels for the EnKF-Inf-Loc, WCEnKF-Inf-Loc,WCEnKF-Inf, WCEnKF and EnKF assimilation schemes.

https://doi.org/10.5194/hess-2019-696
Preprint. Discussion started: 3 February 2020

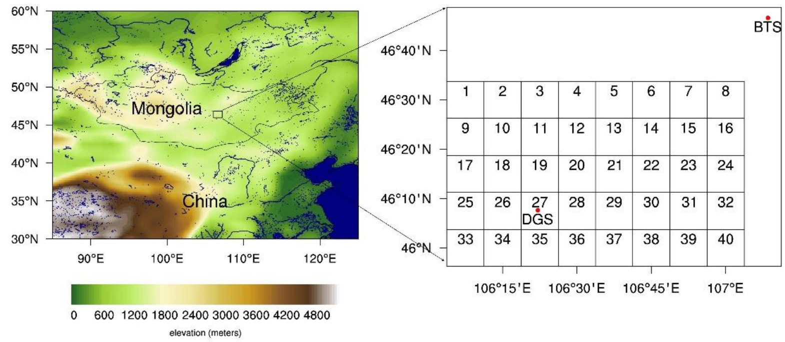

Figure 1. The topography and river distribution (left plot) and the geographical location of the synthetic study area and the two application stations, the DGS and the BTS (right plot).

https://doi.org/10.5194/hess-2019-696
Preprint. Discussion started: 3 February 2020

Hydrology and Earth System Sciences
Discussions

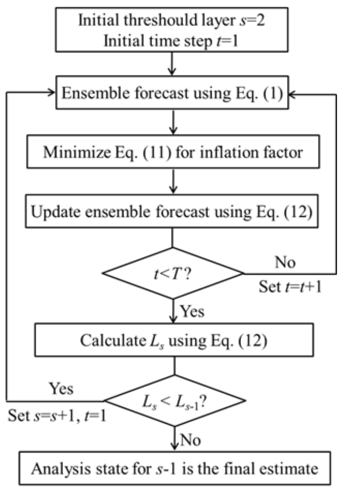

Figure 2. The assimilation procedure and localization scale factor estimation in the experiments. All of the equations are in accordance with that described in the text.

https://doi.org/10.5194/hess-2019-696
Preprint. Discussion started: 3 February 2020

Hydrology and Earth System Sciences
Discussions

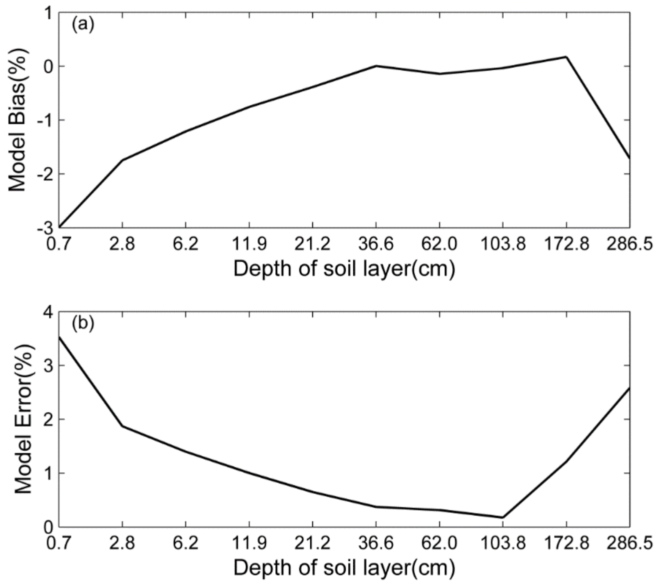

Figure 3. The areal average of the model's bias (a) and error (b) for one step in the soil moisture content between the CoLM and the CLM 4.0. The horizontal axis represents the layer depth.

https://doi.org/10.5194/hess-2019-696
Preprint. Discussion started: 3 February 2020

Hydrology and Earth System Sciences
Open Access
Discussions

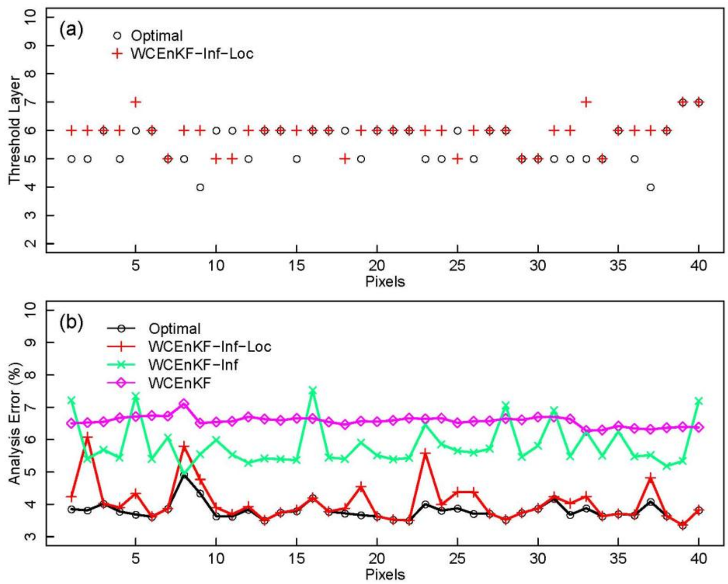

Figure 4. The threshold layers and analysis error for each pixel in the synthetic experiment. Graph (a) illustrates the optimal and WCEnKF-Inf-Loc threshold layers of each pixel. Graph (b) shows the column RSME of each pixel in different schemes with water balance constraint (Optimal, WCEnKF-Inf-Loc, WCEnKF-Inf and WCEnKF). The horizontal axes of (a) and (b) represent the 40 pixels in the study domain.

https://doi.org/10.5194/hess-2019-696
Preprint. Discussion started: 3 February 2020

Hydrology and Earth System Sciences
Open Access
Discussions

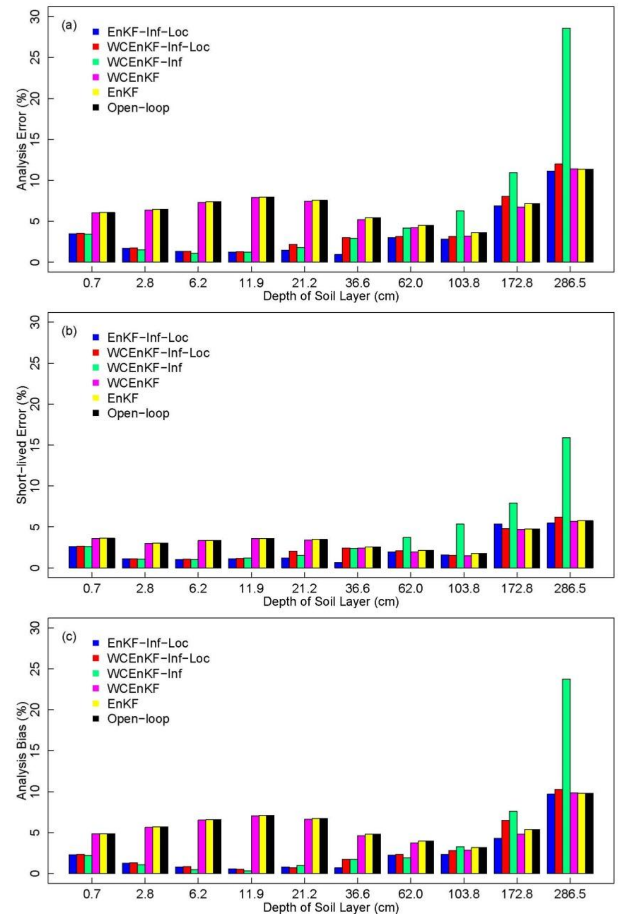

Figure 5. The assimilation results in each layer for an ensemble Kalman filter with forecast error inflation and vertical localization (EnKF-Inf-Loc), a weakly constrained ensemble Kalman filter with forecast error inflation and vertical localization (WCEnKF-Inf-Loc), a weakly constrained ensemble Kalman filter with forecast error inflation (WCEnKF-Inf), a weakly constrained ensemble Kalman filter (WCEnKF), traditional assimilation (EnKF) and an open-loop simulation. Graphic (a) is for spatial averaged analysis error of the soil moisture content, (b) is for the short-lived error and (c) is for the analysis bias.

https://doi.org/10.5194/hess-2019-696
Preprint. Discussion started: 3 February 2020

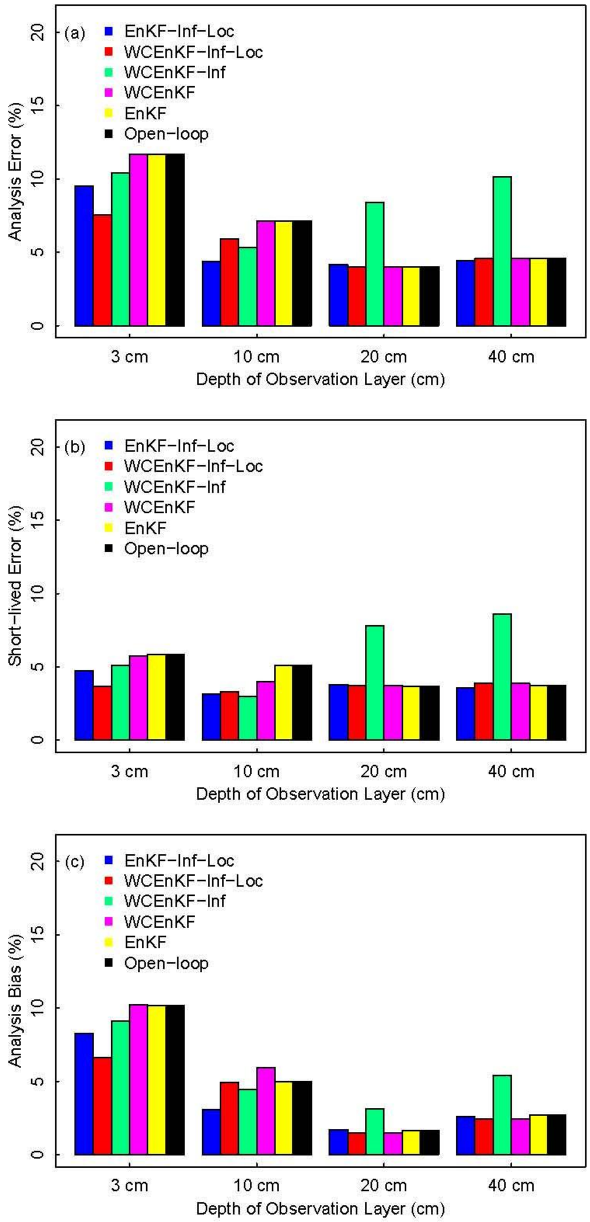

Figure 6. The assimilation results in each observation layer for an ensemble Kalman filter with forecast error inflation and vertical localization (EnKF-Inf-Loc), a weakly constrained ensemble Kalman filter with forecast error inflation and vertical localization (WCEnKF-Inf-Loc), a weakly constrained ensemble Kalman filter with

forecast error inflation (WCEnKF-Inf), a weakly constrained ensemble Kalman filter (WCEnKF), traditional assimilation (EnKF) and an open-loop simulation. Graphic (a) is for spatial averaged analysis error of the soil moisture content, (b) is for the short-lived error and (c) is for the analysis bias.

Hydrology and Earth System Sciences
Discussions

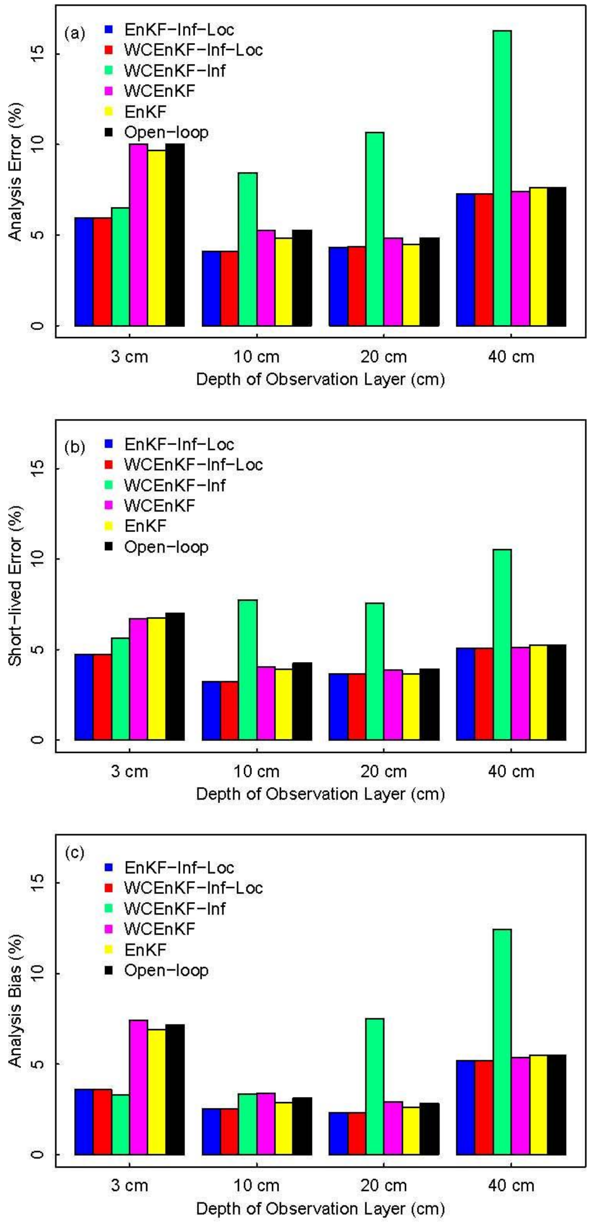

Figure 7. Same as Figure 6, but for BTS station.

https://doi.org/10.5194/hess-2019-696
Preprint. Discussion started: 3 February 2020

Hydrology and Earth System Sciences
Discussions

967 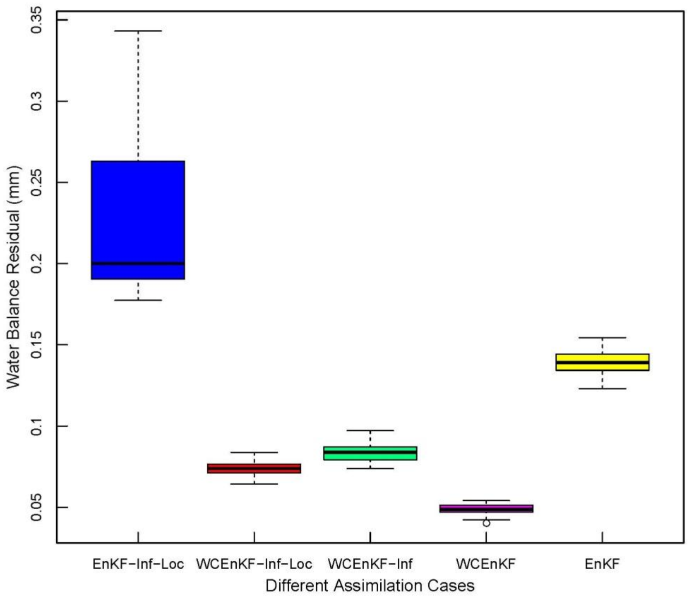

968 Figure 8. The box plot of the water balance residual in all 40 pixels for the
969 EnKF-Inf-Loc, WCEnKF-Inf-Loc,WCEnKF-Inf, WCEnKF and EnKF assimilation
970 schemes.
971

https://doi.org/10.5194/hess-2019-696
Preprint. Discussion started: 3 February 2020

Hydrology and Earth System Sciences
Open Access
EGU
Discussions

Table 1. The node depths (cm) of the 10 soil layers in the CoLM model.

Layer	1	2	3	4	5	6	7	8	9	10
Depth (cm)	0.7	2.8	6.2	11.9	21.2	36.6	62.0	103.8	172.8	286.5

Table 2. Estimated localization scale factor for different cases.

Layer	2	3	4	5	6	7	8	9	10
μ_s	0.2824	0.1256	0.0587	0.0300	0.0163	0.0093	0.0053	0.0025	0.0001